Diagn Interv Radiol 2013; 19:304–311

ABDOMINAL IMAGING
PICTORIAL ESSAY

Subtypes of renal cell carcinoma: MRI and pathological features

Safiye Gürel, Vamsi Narra, Khaled M. Elsayes, Cary Lynn Siegel, Zongming Eric Chen, Jeffrey J. Brown

ABSTRACT
Renal cell carcinoma (RCC) is the most common malignant tumor involving the kidney. Determining the subtypes of renal cell carcinoma is among the major goals of preoperative radiological work-up. Among all modalities, magnetic resonance imaging (MRI) has several advantages, such as inherent soft tissue contrast, detection of lipid and blood products, and excellent sensitivity to detect small amounts of intravenous contrast, which facilitate the discrimination of subtypes of RCC. In this article, we review MRI and pathological features used for determining the main histologic subtypes of RCC, including clear cell, papillary, collecting duct, chromophobe, multilocular cystic, and unclassified RCC.

Renal cell carcinoma (RCC) is the most common malignant epithelial tumor of the kidney, accounting for 85%–90% of all solid renal tumors in adults and comprising 1%–3% of all malignant visceral neoplasms (1). Approximately 40% of patients with RCC eventually die from progression of this disease, making it the most lethal urologic malignancy (2). Today, most RCC instances are incidental masses identified on imaging studies performed for nonurological reasons.

Percutaneous biopsy is a minimally invasive method, and its accuracy for identifying renal tumors ranges from 70% to 90% (3, 4). However, widespread use of percutaneous biopsy remains controversial due to the potential complications of biopsy, the possibility of sampling errors, the dependence on an adequate biopsy sample for analysis, and concerns about how the biopsy information might alter the treatment plan (5). Therefore, histopathological characterization of renal masses with magnetic resonance imaging (MRI) compared with percutaneous biopsy becomes more advantageous.

Determining subtypes of RCC has significant prognostic and therapeutic implications for patients who are poor surgical candidates, for patients who have a metastatic disease, for surgical planning in patients who are surgical candidates, and for immunotherapy and use of the tyrosine kinase inhibitors “sunitinib” and “sorafenib” for clear cell RCC and “temsirolimus” for papillary RCC (6–9).

The need for a different approach to the management of RCC among classical surgical procedures has arisen. Nephron-preserving surgical methods, cryoablation, radiofrequency ablation, targeted molecular therapy or follow-up, and MRI are believed to surpass other modalities both in the diagnosis of RCC and determination of its subtypes (10, 11).

In this article, we review MRI findings and pathological features used for determining the main histologic subtypes of RCC, including clear cell carcinoma, papillary, collecting duct, chromophobe, multilocular cystic, and unclassified RCC.

The role of MRI in renal imaging

There are three indispensable components of renal MRI: breathhold imaging, three-dimensional (3D) gradient echo pulse sequence, and fat detection techniques.

Breathhold imaging is one of the essential techniques in renal mass MRI protocols. Suspended expiration eliminates respiratory motion artifacts and improves registration for subtraction postprocessing. MRI techniques with rapid acquisition times, such as the fast imaging technique and single-shot pulse sequences, are now widely available and very effective with suspended respiration (12). The speed of these se-

From the Department of Radiology (S.G. ✉ *safiyegurel@hotmail.com*), Abant İzzet Baysal University School of Medicine, Bolu, Turkey; Mallinckrodt Institute of Radiology (S.G., V.N., C.L.S.), Washington University School of Medicine, St. Louis, Missouri, USA; University of Texas M.D. Anderson Cancer Center (K.M.E.), Houston, Texas, USA; the Department of Pathology (Z.E.C.), Geisinger Medical Center, Danville, Pennsylvania, USA; the Department of Radiology (J.J.B.), University of St. Louis, St. Louis, Missouri, USA

Received 25 November 2012; accepted 27 November 2012.

Published online 21 February 2013
DOI 10.5152/dir.2013.147

quences allows dynamic contrast-enhanced (DCE) MRI with or without fat suppression (13).

The 3D gradient echo sequence permits dynamic and volumetric imaging under breathhold (14). Image postprocessing with multiplanar reformatting, maximum intensity projection, and volume rendering is often used to assess the relationship between the tumor and vascular system. Subtraction is useful for maximum intensity projection, volume rendering, and determining the contrast enhancement of any mass high on T1 or tiny structures, such as the septa or mural components of a lesion. The 3D gradient echo sequence has decreased the total imaging time because it is no longer necessary to obtain postcontrast images in an additional plane. It also eliminates the need for magnetic resonance angiography sequences. For DCE imaging, interrogation of tumor signal intensity before, during, and after the intravenous administration of a bolus of contrast is possible. The accumulation of the contrast agent in the tumor over time can be used to extract both qualitative and quantitative information regarding the functional integrity of tumor microvasculature (15).

The detection of fat is critical in characterizing renal masses (16, 17). Macroscopic fat is assessed using frequency-selective fat suppression techniques (18), while microscopic fat, i.e., intracytoplasmic vacuoles containing lipids, is assessed using chemical shift imaging, which is available only with gradient-echo imaging (19). The presence of intratumoral lipids results in a decrease in signal intensity on T1-weighted, opposed-phase images compared with the in-phase images in the non-necrotic "viable" tumor (20).

Diffusion-weighted imaging (DWI), an innovative technology for renal masses, is a vital component of renal imaging. DWI provides quantification of the Brownian motion of water molecules in tissues, which depends on tissue organization, cellularity, the integrity of cell membranes, and extracellular space tortousity (21). Qualitative and quantitative information are obtained regarding tissue characterization without the need for gadolinium chelates and alternative imaging for renal lesion characterization in patients at risk for nephrogenic systemic fibrosis (21–24). Few studies have evaluated the correlation of apparent diffusion coefficient (ADC) values with nuclear grade, histological subtype, and cellularity of RCC. However, it is an evolving technology, and as recommended in the literature, it may improve tissue characterization when findings are interpreted along with the findings of conventional MRI sequences (25, 26).

Pathological features of subtypes of RCC

RCC is a group of malignancies arising from tubular epithelium. The classification of RCC has been revised due to advances in correlative, genetic, and histologic studies of both sporadic and familial tumors (27, 28). The World Health Organization working group on tumors of the urinary system and male genital organs proposed the classification in 2004 (29).

RCC is considered a clinicopathologically heterogeneous disease that can be classified into clear cell, papillary, chromophobe, collecting duct carcinoma, medullary carcinoma, multilocular cystic and unclassified (4%–5%) categories that can be histologically differentiated mostly with hematoxylin-eosin staining techniques (29). Some RCCs undergo sarcomatoid or rhabdoid dedifferentiation, a process thought to represent the high-grade end of all subtypes (29, 30).

MRI findings of RCC subtypes

Clear cell carcinoma

Clear cell carcinoma is the most common type of RCC, accounting for 70% of all RC. They are predominantly sporadic (95%) but can be familial or associated with Von Hippel Lindau disease. Up to 96% of clear cell RCCs are associated with 3p deletions, including somatic inactivating mutations of the von Hippel Lindau gene (31).

Clear cell RCC recapitulates the epithelium of the proximal convoluted tubules (32). At histologic analysis, clear cell RCC is composed of cells with optically clear cell cytoplasm due to accumulation of dissolved lipids and cholesterol. These tumors often contain cells with granular eosinophilic cytoplasm. Tumor cells are characteristically arranged in sheets, acini, or alveoli, and prominent thin-walled vasculature is characteristic (33). Hyalinization, fibrosis, and coagulative tumor necrosis are common, while cystic degeneration occurs in 4%–15% of RCCs (34). They are predominantly hypervascular tumors and the microvessel density is higher than other subtypes of RCC (35).

Clear cell RCC has a relatively unfavorable prognosis, with a five-year survival of 50%–60%, which is less favorable than other RCC subtypes, with the exception of the collecting duct carcinoma subtype (33). Compared with papillary and chromophobe RCC, they tend to be symptomatic more commonly, present at an advanced stage and have a higher rate of metastasis (36). Sarcomatoid, and rhabdoid differentiations of clear cell RCC are also associated with a poorer prognosis.

Clear cell carcinoma displays common MRI characteristics of RCC. They originate from the renal cortex and typically exhibit an expansile growth pattern. Multicentricity and bilaterality are rare (5%) in sporadic cases. They frequently have a signal intensity similar to that of the renal parenchyma on T1-weighted images and increased signal intensity on T2-weighted images. Necrosis, hemorrhage and cysts are the main causes of varying appearances on MRI. Central necrosis is common and typically considered a homogeneous hypointense area in the center of the mass on T1-weighted images. On T2-weighted images, necrosis tends to have a moderate to high signal intensity, although it may occasionally appear hypointense (Fig. 1a). In the presence of central necrosis, a solid rim of tumor is frequently observed at the periphery of the mass. Postcontrast images demonstrate a lack of enhancement in areas of necrosis and marked enhancement in the viable components of the tumor (Fig. 1b) (37).

Intratumoral hemorrhage may occur and has a variable appearance depending at the stage of degradation of the component blood products. Subacute to chronic hemorrhage generally demonstrates a high signal intensity in both T1- and T2-weighted images. Long-standing hemorrhage, which predominantly contains hemosiderin,

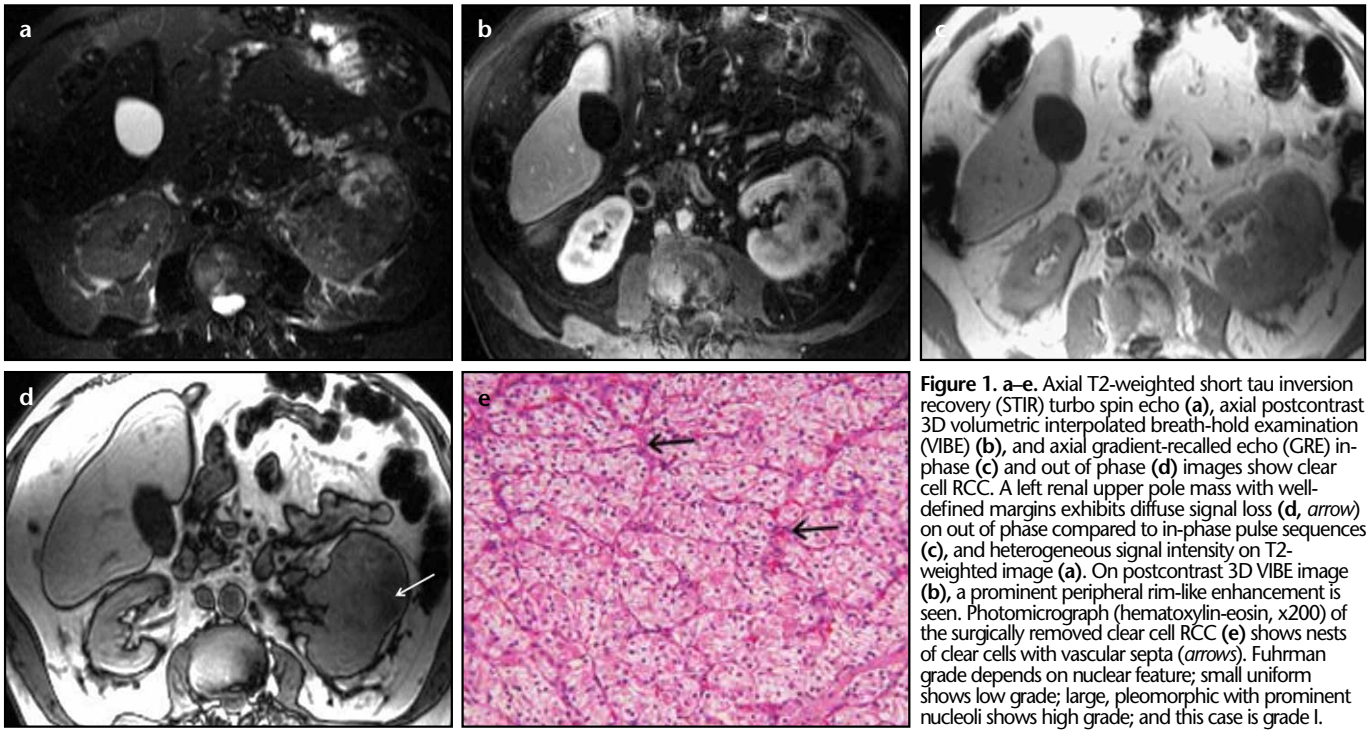

Figure 1. a–e. Axial T2-weighted short tau inversion recovery (STIR) turbo spin echo **(a)**, axial postcontrast 3D volumetric interpolated breath-hold examination (VIBE) **(b)**, and axial gradient-recalled echo (GRE) in-phase **(c)** and out of phase **(d)** images show clear cell RCC. A left renal upper pole mass with well-defined margins exhibits diffuse signal loss **(d,** *arrow*) on out of phase compared to in-phase pulse sequences **(c),** and heterogeneous signal intensity on T2-weighted image **(a).** On postcontrast 3D VIBE image **(b),** a prominent peripheral rim-like enhancement is seen. Photomicrograph (hematoxylin-eosin, x200) of the surgically removed clear cell RCC **(e)** shows nests of clear cells with vascular septa (*arrows*). Fuhrman grade depends on nuclear feature; small uniform shows low grade; large, pleomorphic with prominent nucleoli shows high grade; and this case is grade I.

is typically hypointense in both T1- and T2-weighted images (38).

Considerable loss of signal intensity within the solid portions of clear cell RCCs on opposed phase images compared with in-phase images is due to cytoplasmic fat and has been detected in up to 60% of clear cell RCC (Fig. 1c–e) (39).

Clear cell RCC is mostly hypervascular, which has been ascribed to inactivation of tumor suppressor genes (such as the von Hippel Lindau gene) and subsequent elaboration of vascular and other growth factors (40). In contrast-enhanced MRI with heterogenous enhancement in the arterial phase continuing with or without washout (37), the degree of contrast enhancement may help distinguish clear cell RCC from non-clear cell subtypes. Sun et al. (41) reported the results of region-of-interest measurements within tumor and uninvolved renal cortex, which were used to calculate percentage signal intensity change and tumor-to-cortex enhancement index. On both the corticomedullary and nephrographic phase images, clear cell RCCs showed a greater signal intensity change (205.6% and 247.1%, respectively) than papillary RCCs (32.1% and 96.6%, respectively). The tumor-to-cortex enhancement indexes at the corticomedullary and nephrographic phases were largest for clear cell RCCs (1.4 and 1.2) compared with indexes of papillary and chromophobe RCC. Signal intensity changes on corticomedullary phase images are the most effective parameter for distinguishing clear cell and papillary RCC; a threshold value of 84% permitted distinction with 93% sensitivity and 96% specificity. Vargas et al. (42) examined the quantitative region of interest analysis of tumor enhancement patterns at multiphase MRI. They showed that in three postcontrast phases (corticomedullary, nephrographic, and excretory), the percentage change in signal intensity relative to the precontrast phase was significantly greater in clear cell carcinoma (230%, 250%, and 227% for corticomedullary, nephrographic, and excretory phases, respectively) compared with papillary and chromophobe RCC.

A hypointense rim or pseudocapsule might be observed on both T1- and T2-weighted images and is thought to be related to compression of the adjacent renal parenchyma by the expanding tumor, although a fibrous capsule can occasionally be observed at pathologic analysis. The interruption of this pseudocapsule correlates with advanced stage (invasion of perirenal fat) and higher nuclear grade (43).

In the case of DWI, Goyal et al. (26) showed that the mean ADC value of clear cell RCC was found to be significantly higher than that of non-clear cell RCC, with an optimal cut-off ADC value of 1.4904×10^{-3} mm^2/s. Taouli et al. (25) and Wang et al. (24) reported similar results for clear cell RCC, while Sandrasegaran et al. (44) did not find any significant difference in the ADC values of clear cell RCCs and non-clear cell malignancies.

Papillary cell carcinoma

This subtype accounts for 10%–15% of all RCC (29). It may be sporadic or familial. Tumor epithelium is reminiscent of the epithelium of the proximal convoluted tubules (32). Histologically, it is characterized by a papillary growth pattern and occurs in both sporadic and familial forms. The cells covering the papillae range from small to large and have a variable cytoplasmic staining. Psammoma bodies and edema are common in the papillary cores. The most striking feature is the foamy histiocytic infiltration into the interstitium of the lesion, which is laden with fat and hemosiderin. Hemosiderin is also observed in the tumor cells (17). There are two histomorphologic subtypes of papillary RCC. Type 1 tumors are characterized by a monolayer

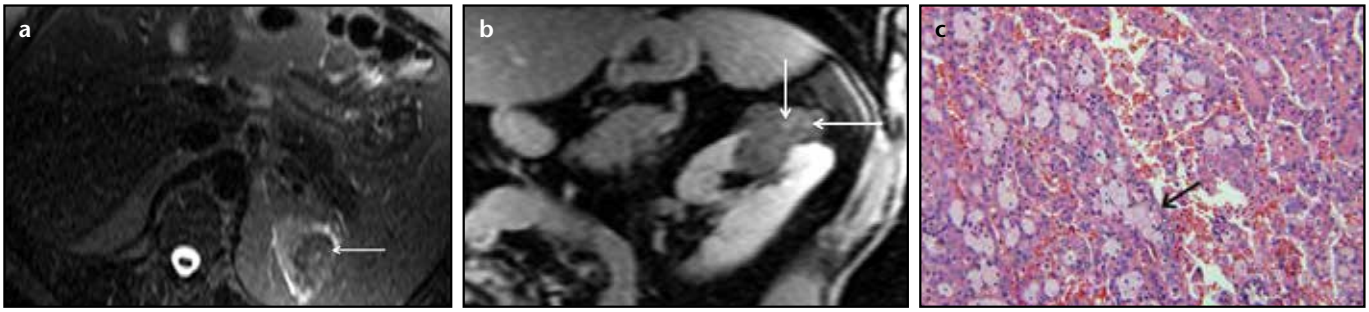

Figure 2. a–c. Axial T2-weighted STIR turbo spin echo **(a)** and oblique sagittal postcontrast 3D VIBE **(b)** images show papillary RCC. A left renal upper pole mass with well-defined margins is hypointense on T2-weighted image **(a,** *arrow***)**. On postcontrast image **(b)** there is minimal faint, irregular, spot-like enhancing foci (*arrows*) within the lesion with no considerable washout. Photomicrograph (hematoxylin-eosin, x200) of the surgically removed papillary RCC **(c)** shows papillae formation (*arrow*) with numerous pale stained histiocytes.

of small cells with scanty cytoplasm, while type 2 tumors contain high nuclear grade cells with abundant eosinophilic cytoplasm (29).

The most common cytogenetic abnormalities are trisomies of chromosomes 3, 7, 12, 16, 17, and 20 and loss of the Y chromosome and *c-MET* mutations of a subset of sporadic papillary RCC (45, 46). Cytogenetic features support the diagnosis of papillary RCC even when the papillary pattern is not prominent.

Papillary RCC has a better prognosis than clear cell RCC, with a five-year survival rate of approximately 90% and often presenting at an early stage (33, 36). Type 1 papillary RCC is typically of a lower stage and grade than type 2 tumors and is thus associated with a better prognosis (29).

Papillary RCC tend to be solid, large, well-defined, and slow-growing tumors (46). They frequently exhibit bilaterality (4%) and/or multifocality (22.5%) more than other RCC subtypes and display distinct MRI features (36). Approximately 70% are intrarenal at presentation. They are small in size and hypointense compared with the cortex on T2-weighted images and have homogeneous signal intensity (Fig. 2a). Hypointensity on T2-weighted images has often been assigned to the hemosiderin deposition, hemorrhage, or necrosis of the tumor. Hypointensity can still be present in the absence of these contents and provides an accurate distinction from clear cell RCC, which typically exhibits heterogeneously increased signal intensity on T2-weighted images (11). A fibrous capsule is typically present in papillary RCCs. Larger tumors show heterogeneity due to necrosis, hemorrhage, and calcification. The overall sensitivity and specificity of MRI in predicting the histologic subtype is reported to be 92% and 83% for clear cell RCC and 80% and 94% for papillary RCC, respectively (47). Sarcomatoid dedifferentiation may be observed in approximately 5% of cases.

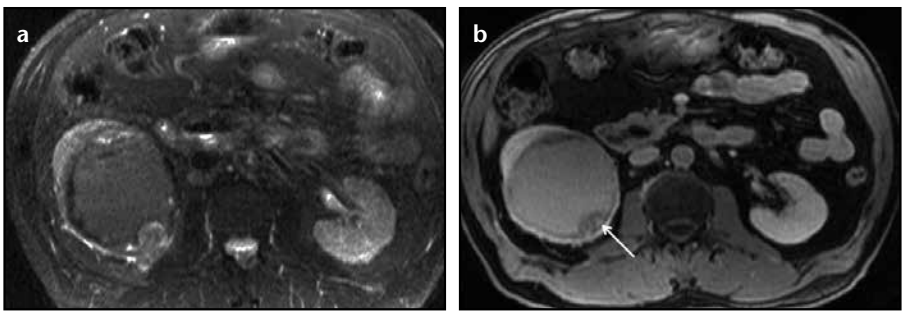

Figure 3. a, b. Axial T2-weighted STIR turbo spin echo **(a)** and axial postcontrast VIBE **(b)** images show a rhabdoid variant of papillary RCC. A huge hemorrhagic right renal lower pole mass with solid mural component is observed **(a, b)**. There is heterogeneous signal intensity on T2-weighted image **(a)**. On postcontrast images there is minimal heterogenous enhancement of the mural nodule **(b,** *arrow).*

Papillary carcinoma, either the primary tumor or its metastases, has been shown to contain microscopic fat that is detectable with chemical shift imaging (29). The major difference in fat content between clear and papillary cell carcinoma is the localization of fat, which can only be defined pathologically. Fat is present in the interstitial histiocytes of papillary cell carcinoma rather than tumor cells such as in clear cell carcinoma (29). Although extremely rare, the presence of macroscopic fat (corresponding histologically to cholesterol-laden macrophages) has also been reported (48).

Papillary RCC shows hypo- or avascularity on angiography. Due to hypovascularity, they tend to enhance minimally on cortical phase and seem hypointense compared with renal parenchyma on the nephrographic phase. On postcontrast series, they enhance homogenously, or small, curvilinear enhancing structures can be detected within the tumor (Fig. 2b, 2c) (11). Papillary RCC might also present as cystic neoplasms with hemorrhagic content and peripheral-enhancing solid papillary projections (Fig. 3a, 3b). Sun et al. (41) reported that the tumor-to-cortex enhancement indexes at corticomedullary and nephrographic phases were the smallest for papillary RCCs among clear cell and chromophobe RCC. Percentage signal intensity changes on corticomedullary phase images were found to be the most effective parameter for distinguishing clear cell and papillary RCC; a threshold value of 84% permitted distinction with 93% sensitivity and 96% specificity. Vargas et al. (42) reported similar results with region of interest measurements in all three postcontrast phases. In corticomedullary, nephrographic, and excretory phases, the percentage change in signal intensity relative to the pre contrast phase was significantly lower in papillary carcinoma (49%, 92%, and 88% for corticomedullary, nephrographic, and excretory phases) compared with clear cell and chromophobe RCC.

Taouli et al. (25), Goyal et al. (26), and Wang et al. (24) reported low mean ADC values for papillary RCC compared with clear cell RCC, while no significant difference was detected compared with chromophobe RCC. However, Sandrasegaran et al. (44) did not find any significant difference in the ADC values of clear cell RCCs and non-clear cell malignancies. In papillary RCC, cells are organized into papillary projections. Its compact tissue architecture and higher nuclear cytoplasmic ratio (49) might be responsible for lower ADC values.

Chromophobe RCC

Among all RCC subtypes, chromophobe RCC is the third most common subtype and accounts for approximately 4%–11% of RCCs (29). Chromophobe RCC shows a mean age of incidence in the 6th decade. Men and women are equally affected.

Chromophobe RCC is postulated to arise from the intercalated cells of the renal cortex. Histologically, tumor cells are round to polygonal and have well-defined cytoplasm borders, pale eosinophilic cytoplasm with a fine reticular pattern, and perinuclear haloes (33). Tumor cells usually demonstrate a pattern of solid growth. Cytogenetically multiple monosomy (1, 2) and hypodiploidy is associated with chromophobe RCC (29, 32, 45).

This tumor type has the best prognosis among the RCC categories. Metastasis occurred in approximately 7.1% of patients, and 3%–6% died of chromophobe RCC. The reported five-year survival is approximately 78%–92% (33, 36).

MRI features of chromophobe RCC can be identical to those of clear cell RCC. They might appear hypointense on T2-weighted images compared with renal parenchyma (Fig. 4a). Cystic changes can be observed within a solid tumor, and central necrosis might be absent, even in very large chromophobe carcinomas (50). Signal loss on out of phase images due to microscopic fat has been reported (51). It is interesting that oncocytomas and chromophobe RCC share similar ontogenic and histologic features (on hematoxylin-eosin-stained slides) and some imaging findings. Oncocytomas develop from type B intercalated cells of the cortical collecting duct and are indistinguishable from chromophobe RCC on imaging studies, sharing features such as central scar and spoke wheel pattern of enhancement (51) .

Chromophobe RCC is the second most common hypovascular tumor after papillary RCC. Despite its large size, chromophobe RCC demonstrates relatively homogeneous enhancement compared with papillary RCC (Fig. 4b–d). Sun et al. (41) reported that chromophobe RCC showed an intermediate change in both percentage signal intensity (109.9% and 192.5%) and tumor-to-cortex enhancement indexes at corticomedullary and nephrographic phases (0.6 and 0.8, respectively), which is lower than clear cell RCC and higher than papillary RCC. Vargas et al. (42) reported similar results, showing that chromophobe RCC displayed significantly less enhancement than clear cell carcinoma at all three postcontrast phases.

In chromophobe RCC, cells are arranged in solid sheets. Its compact tissue architecture and dense cytoplasm may cause lower ADC values. Wang et al. (24) showed a significantly higher mean ADC of clear cell RCC (1.849×10^{3} mm^2/s) than papillary (1.087×10^{-3} mm^2/s) and chromophobe (1.307×10^{-3} mm^2/s) RCC. However, there was no significant difference in the ADC values of papillary and chromophobe RCC. Goyal et al. (26) also reported similar results.

Collecting duct carcinoma

Collecting duct carcinoma is rare, accounting for less than 1% of cases, and an aggressive RCC subtype. The mean age of patients with collecting duct carcinoma is mid-50s, and the male-to-female ratio is approximately 2:1. This carcinoma has a very unfavorable prognosis because one-third of the patients have distant metastasis at diagnosis, and two-thirds of patients die within two years (39).

Collecting duct carcinoma is thought to originate in the distal segment of the collecting duct in the renal medullary pyramids and is histologically characterized by tubular or tubulopapillary growth patterns, the presence of inflammatory or desmoplastic stroma, and mucin production (52). Cytogenetically, the loss of multiple chromosomes (1, 6, 14, 15, 22) and gain of chromosome 3 have been detected (45).

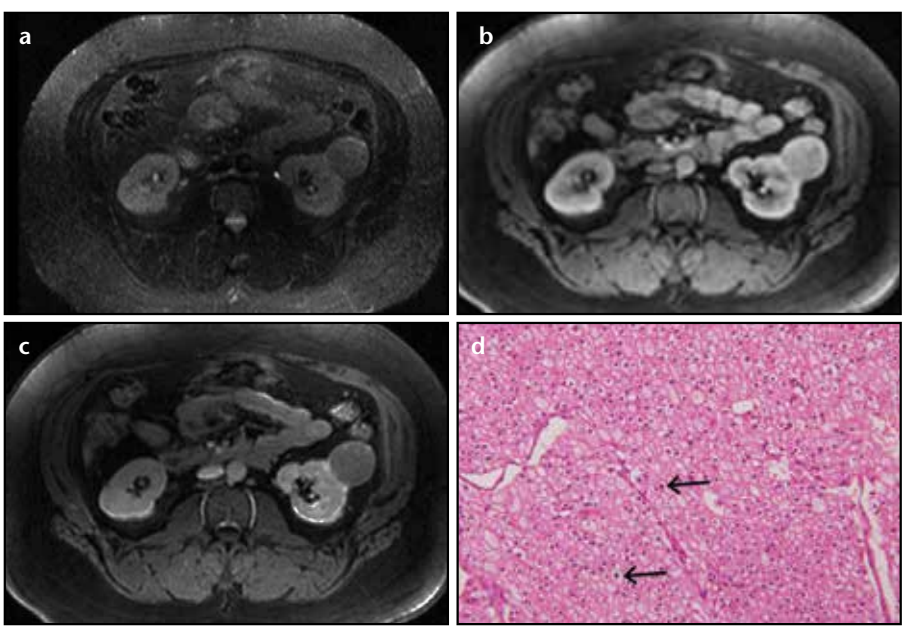

Figure 4. a–d. Axial T2-weighted STIR turbo spin echo **(a)**, axial postcontrast cortical and nephrographic phase 3D VIBE **(b, c)** images show chromophobe RCC. A left cortical, exophytic, interpolar renal mass is homogeneous and moderately hypointense on T2-weighted image **(a)**. The lesion enhances homogenously, and there is apparent washout on postcontrast nephrographic phase images **(b, c).** Photomicrograph (hematoxylin-eosin, x200) of the surgically removed tumor **(d)** shows cells with central clearing, irregular nuclear contours, and high-grade nuclear features (*arrows*).

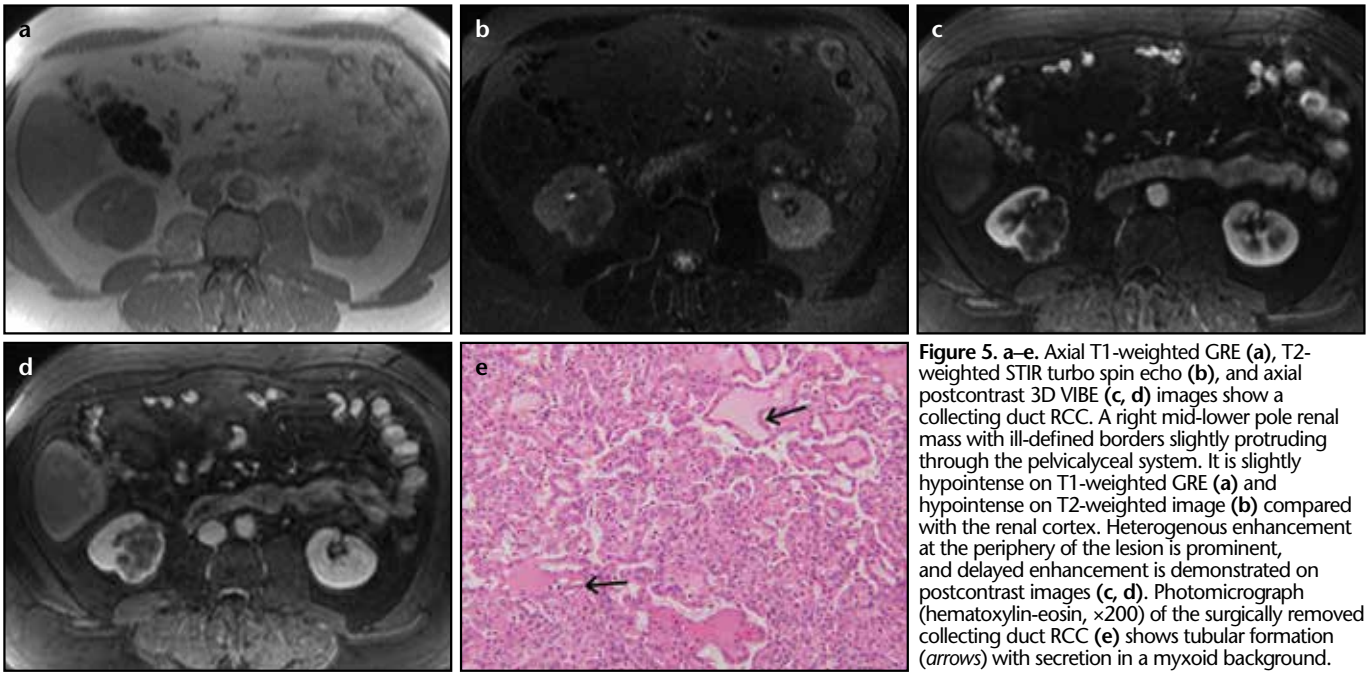

Figure 5. a–e. Axial T1-weighted GRE **(a)**, T2-weighted STIR turbo spin echo **(b)**, and axial postcontrast 3D VIBE **(c, d)** images show a collecting duct RCC. A right mid-lower pole renal mass with ill-defined borders slightly protruding through the pelvicalyceal system. It is slightly hypointense on T1-weighted GRE **(a)** and hypointense on T2-weighted image **(b)** compared with the renal cortex. Heterogenous enhancement at the periphery of the lesion is prominent, and delayed enhancement is demonstrated on postcontrast images **(c, d)**. Photomicrograph (hematoxylin-eosin, ×200) of the surgically removed collecting duct RCC **(e)** shows tubular formation (*arrows*) with secretion in a myxoid background.

On MRI, collecting duct carcinoma have variable signal intensity on T1-weighted and frequent hypointensity on T2-weighted images (Fig. 5a, 5b) (53). They may appear heterogeneous, with areas of necrosis, hemorrhage, and calcification and a cystic component can be observed in 50% of patients. They are hypovascular tumors angiographically and display heterogeneous or predominantly peripheral contrast enhancement (Fig. 5c–e). The epicenter of these tumors is typically located in the medullary portion of the kidney near the region of the pelvis. However, almost all tumors exhibit focal cortical extension, and some even exhibit perirenal extension (54). They have a tendency to display infiltrative patterns, preserving renal contour rather than an expansile growth. This infiltrative appearance may be difficult to detect when the lesion is large or has an expansile component and differentiation from clear cell RCC is not possible (54).

Although it could be classified as a non-clear cell type and be expected to have lower ADC compared with clear cell RCC, there is a lack of data specific for collecting duct type RCC in both DCE MRI and DWI.

Unclassified RCC

This is a diagnostic category for RCC that does not fit readily into any other category and is a diagnosis of exclusion. It accounts for 4%–5% of RCC subtypes.

Tumors in this category are histologically heterogeneous and most often of high grade. There are some features that may help identify a tumor as unclassified: sarcomatoid cells without recognizable epithelial elements, mucin production, mixtures of epithelial and stromal elements, and unrecognizable cell types (33). This category has the worst prognosis among RCC subtypes (29, 36).

There is little information about MRI findings of this subtype. When heterogenous histological features are taken into consideration, MRI findings likely display a wide spectrum. They may be solid with a cystic component, hyperintense on T1- and isointense on T2-weighted images, show heterogenous enhancement and contain hemorrhage (Fig. 6a–d) (55). Unclassified RCCs display significantly smaller mean signal intensity changes than clear cell carcinoma at three postcontrast phases (42). Although it is classified as non-clear cell type and expected to have lower ADC than clear cell RCC, there is a lack of data specific for unclassified RCC in DWI.

Multilocular cystic RCC

This is a rare entity with an incidence varying between 1%–4% of all RCC (56). Multilocular cystic RCC is found in adults aged 20–76 years, with a mean age of 51 years, and observed predominantly in males (male:female, 3:1) (57). Multilocular cystic RCC is characterized by septated, variable-sized cysts separated from the kidney by a fibrous capsule (58). If treated early, multilocular cystic RCC has an excellent prognosis and may be permanently cured. Recurrence and metastasis have not yet been reported (58).

Histopathologic analysis demonstrates serous, gelatinous, or hemorrhagic cysts lined by a monolayer of epithelial cells with clear cytoplasm (1). These cells, consisting of clear cytoplasm, form small collections but do not form expansile nodules, which is an important differential criterion to distinguish multilocular cystic RCC from clear cell RCC with extensive cystic change (57). Calcification can be found in the septa or pseudocapsule of more than 20% of multilocular cystic RCC.

On MRI, multilocular cystic RCCs typically manifest as multilocular cystic tumors. They have a variable imaging pattern, with a Bosniak category ranging from IIF to IV. As multilocular cystic RCC lesions increase in complexity on images (higher Bosniak category), there is a corresponding increase in the volume of malignant cells lining the tumor and an increase in the presence of vascularized fibrous tissue (59). On

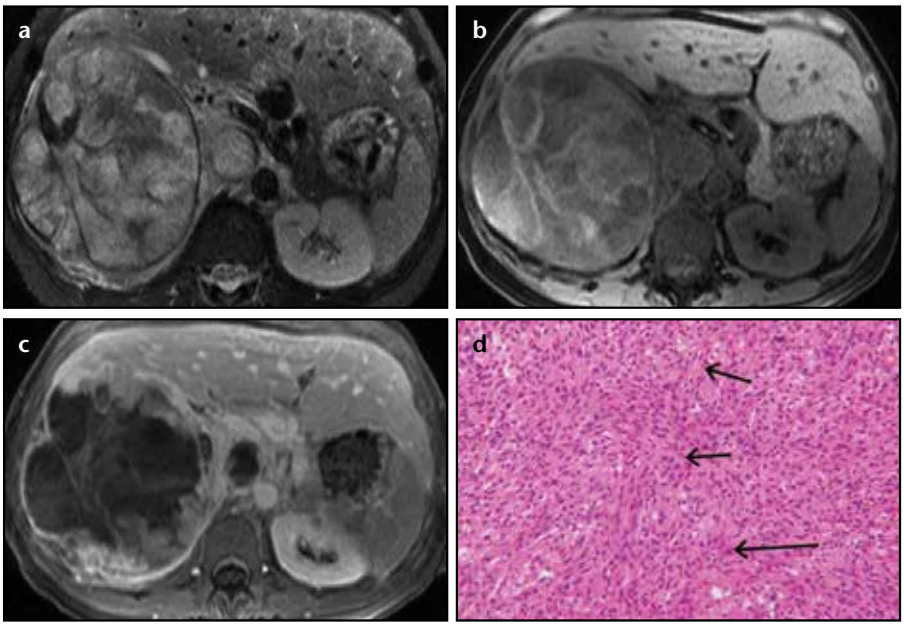

Figure 6. a–d. Axial T2-weighted STIR turbo spin echo **(a)**, axial pre- **(b)**, and postcontrast **(c)** 3D VIBE images show an unclassified RCC. A complex, predominantly cystic, right upper pole renal mass is observed **(a)**. On pre- and postcontrast images **(b, c)**, thick enhancing septa and solid mural components are visualized within the lesion. Invasion of perirenal fat and thrombosis of the inferior vena cava are accompanying findings with the lesion **(c)**. Photomicrograph (hematoxyline-osin, ×200) of the surgically removed tumor **(d)** shows pindle cells (*short arrows*) with nuclear pleomorphism and mitosis (*long arrow*).

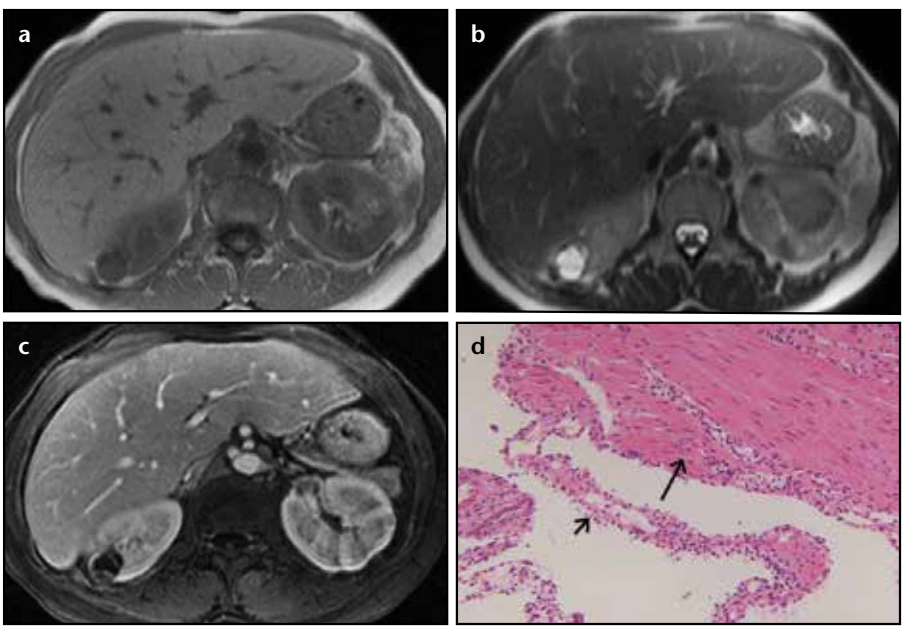

Figure 7. a–d. Axial T1-weighted **(a)**, T2-weighted STIR turbo spin echo **(b)**, and axial nephrographic phase on postcontrast 3D VIBE **(c)** images show multilocular cystic RCC. The lesion is hypointense on T1-weighted **(a)** and hyperintense on T2-weighted **(b)** images consisting a speckle of signal loss that may indicate hemosiderin within the lesion. A cortical cystic lesion with a few enhancing septa, which is an alerting sign of malignancy, is demonstrated **(c)**. Photomicrograph (hematoxylin-eosin, ×200) showing cystic walls lined by cuboidal cells (*long arrow*) with universal small round nuclei and clear cytoplasm **(d)**. Small nests of tumor cells with similar morphology are also evident in the fibrotic septa (*short arrow*).

T1- and T2-weighted images, they frequently show hyperintensity, likely due to proteinaceous fluid or hemorrhage, or may display heterogenous signal intensity on both pulse sequences (Fig. 7a, 7b) (59). Blood products of different ages may create various signal intensities. On post contrast series, there is minimal internal, asymmetric septal, or wall enhancement (Fig. 7c, 7d).

There are not sufficient specific data regarding multilocular cystic RCC in DCE MRI and DWI.

Conclusion

Determining the subtypes of RCC is essential for predicting prognosis and managing theraupetic strategies. In the preoperative radiological work-up, MRI is the best modality for providing important information to diagnose RCC subtypes.

Conflict of interest disclosure

The authors declared no conflicts of interest.

References

1. Pantuck AJ, Zisman A, Belldegrun AS. The changing natural history of RCC. J Urol 2001; 166:1611–1623. [CrossRef]
2. Belldegrun A, deKernion JB. Renal tumors. In: Walsh PC, Retik AB, Vaughan ED Jr, et al. eds. Campbell's urology. 7th ed. Philadelphia: W.B.Saunders, 1998; 2283–2326.
3. Dechet CB, Zincke H, Sebo TJ, et al. Prospective analysis of computerized tomography and needle biopsy with permanent sectioning to determine the nature of solid renal masses in adults. J Urol 2003; 169:71–74. [CrossRef]
4. Silverman SG, Gan YU, Mortele KJ, Tuncali K, Cibas ES. Renal masses in the adult patient: the role of percutaneous biopsy. Radiology 2006; 240:6–22. [CrossRef]
5. Russo P. Partial nephrectomy for renal cancer: part I. BJU Int 2010; 105:1206–1220. [CrossRef]
6. Upton MP, Parker RA, Youmans A, McDermott DF, Atkins MB. Histologic predictors of renal cell carcinoma response to interleukin-2-based therapy. J Immunother 2005; 28:488–495. [CrossRef]
7. Motzer RJ, Hutson TE, Tomczak P, et al. Sunitinib versus interferon alfa in metastatic renal-cell carcinoma. N Engl J Med 2007; 356:115–124. [CrossRef]
8. Escudier B, Eisen T, Stadler WM, et al. Sorafenib in advanced clear cell renal-cell carcinoma. N Engl J Med 2007; 356:125–134. [CrossRef]
9. Dutcher JP, Szczylik C, Tannir N, et al. Correlation of survival with tumor histology, age, and prognostic risk group for previously untreated patients with advanced renal cell carcinoma (adv RCC) receiving temsirolimus (TEMSR) or interferon-alpha (IFN). J Clin Oncol 2007; 25(Suppl 18):5033.
10. Thrasher JB, Paulson DF. Prognostic factors in renal cell cancer. Urol Clin North Am 1993; 20:247–262.
11. Yoshimitsu K, Irie H, Tajima T, et al. MR imaging of renal cell carcinoma: Its role in determining cell type. Radiat Med 2004; 6:371–376.
12. Zhang J, Pedrosa I, Rofsky NM. MR techniques for renal imaging. Radiol Clin N Am 2003; 41:877–907. [CrossRef]

13. Ho VB, Allen SF, Hood MN, Choyke PL. Renal masses: quantitative assessment of enhancement with dynamic MR imaging. Radiology 2002; 224:695–700. [CrossRef]
14. Rofsky NM, Lee VS, Laub G, et al. Abdominal MR imaging with a volumetric interpolated breath-hold examination. Radiology 1999; 212:876–884.
15. Parker GJM, Buckley DL. Tracer kinetic modelling for T1-weighted DCE-MRI. In: Jackson A, Buckley DL, Parker GJM, eds. Dynamic contrast-enhanced magnetic resonance imaging in oncology. 1st ed. Berlin: Springer-Verlag, 2005; 81–92. [CrossRef]
16. Yoshimitsu K, Honda H, Kuroiwa T, et al. MR detection of cytoplasmic fat in clear cell RCC utilizing chemical shift gradient-echo imaging. J Magn Res Imaging 1999; 9:579–585. [CrossRef]
17. Yoshimitsu K, Honda H, Kuroiwa T, et al. Fat detection in granular-cell RCC using chemical shift gradient-echo imaging: another renal tumor that contains fat. Abdom Imaging 2000; 25:100–102. [CrossRef]
18. Mao J, Yan H, Brey WW, et al. Fat tissue and fat suppression. Magn Reson Imaging 1993; 11:385–393. [CrossRef]
19. Outwater EK, Blasbalg R, Siegelman ES, Vala M. Detection of lipid in abdominal tissues with opposed-phase gradient-echo images at 1.5 T: techniques and diagnostic importance. Radiographics 1998; 18:1465–1480.
20. Pedrosa I, Alsop DC, Rofsky NM. Magnetic resonance imaging as a biomarker in RCC. Cancer 2009; 115:2334–2345. [CrossRef]
21. Padhani AR, Liu G, Koh DM, et al. Diffusion-weighted magnetic resonance imaging as a cancer biomarker: consensus and recommendations. Neoplasia 2009; 11:102–125.
22. Kim S, Naik M, Sigmund E, Taouli B. Diffusion-weighted MR imaging of the kidneys and the urinary tract. Magn Reson Imaging Clin N Am 2008;16:585–596. [CrossRef]
23. Thoeny HC, De Keyzer F, Oyen RH, et al. Diffusion-weighted MR imaging of kidneys in healthy volunteers and patients with parenchymal diseases: initial experience. Radiology 2005; 235:911–917. [CrossRef]
24. Wang H, Cheng L, Zhang X, et al. Renal cell carcinoma: diffusion weighted MR imaging for subtype differentiation at 3.0 T. Radiology 2010; 257:135–143. [CrossRef]
25. Taouli B, Thakur RK, Mannelli L, et al. Renal lesions: characterization with diffusion-weighted imaging versus contrast-enhanced MR imaging. Radiology 2009; 251:398–407. [CrossRef]
26. Goyal A, Sharma R, Bhalla AS, et al. Diffusion-weighted MRI in renal cell carcinoma: a surrogate marker for predicting nuclear grade and histological subtype. Acta Radiologica 2012; 53:349–358. [CrossRef]
27. Reuter VE, Presti JC Jr. Contemporary approach to the classification of renal epithelial tumors. Semin Oncol 2000; 27:124–137.
28. Bodmer D, Van den Hurk W, Van Gronigen JJ, et al. Understanding familial and non-familial renal cell cancer. Hum Mol Genet 2002; 11:2489–2498. [CrossRef]
29. Eble JN, Sauter G, Epstein JI, Sesterhenn IA, et al. Pathology and genetics of tumours of the urinary system and male genital organs. In: Kleihues P, Sobin LH, eds. World Health Organization Classification of Tumours. 1st ed. Lyon: IARC Press, 2004; 10–43.
30. Andre M, Helenon O, De Fromont M, et al. Kidney tumors: clinical and pathological findings and detection. J Radiol 2002; 83:773–783.
31. Sukosd F, Kuroda N, Beothe T, Kaur AP, Kovacs G. Deletion of chromosome 3p14.2-p25 involving the VHL and FHIT genes in conventional renal cell carcinoma. Cancer Res 2003; 63:455–457.
32. Polascik TJ, Bostwick DG, Cairns P. Molecular genetics and histopathologic features of adult distal nephron tumors. Urology 2002; 60:941–946. [CrossRef]
33. Cheville JC, Lohse CM, Zincke H, Weaver AL, Blute ML. Comparisons of outcome and prognostic features among histologic subtypes of RCC. Am J Surg Pathol 2003; 27:612–624. [CrossRef]
34. Hayakawa M, Hatano T, Tsuji A, Nakajima F, Ogawa Y. Patients with renal cysts associated with RCC and the clinical implications of cyst puncture: a study of 223 cases. Urology 1996; 47: 643–646. [CrossRef]
35. MacLennan GT, Bostwick DG. Microvessel density in renal cell carcinoma: lack of prognostic significance. Urology 1995; 46:27–30. [CrossRef]
36. Amin MB, Amin MB, Tamboli P, et al. Prognostic impact of histologic subtyping of adult renal epithelial neoplasms: an experience of 405 cases. Am J Surg Pathol 2002; 26:281–291. [CrossRef]
37. Eilenberg SS, Lee JK, Brown J, Mirowitz SA, Tartar VM. Renal masses: evaluation with gradientecho Gd-DTPA-enhanced dynamic MR imaging. Radiology 1990; 176:333–338.
38. Wagner BJ. The kidney: radiologic-pathologic correlation. Magn Reson Imaging Clin N Am 1997; 5:13–28.
39. Outwater EK, Bhatia M, Siegelman ES, Burke MA, Mitchell DG. Lipid in renal clear cell carcinoma: detection on opposed-phase gradient-echo MR images. Radiology 1997; 205:103–107.
40. Cohen HT, McGovern FJ. Renal-cell carcinoma. N Engl J Med 2005; 353:2477–2490. [CrossRef]
41. Sun MR, Ngo L, Genega EM, et al. Renal cell carcinoma: dynamic contrast-enhanced MR imaging for differentiation of tumor subtypes—correlation with pathologic findings. Radiology 2009; 250:793–802. [CrossRef]
42. Vargas HA, Chaim J, Lefkowitz RA, et al. Radiology 2012; 264:779–788. [CrossRef]
43. Yamashita Y, Watanabe O, Miyazaki T, Yamamoto H, Harada M, Takahashi M. Cystic renal cell carcinoma: imaging findings with pathologic correlation. Acta Radiol 1994; 35:19–24. [CrossRef]
44. Sandrasegaran K, Sundaram CP, Ramaswamy R. Usefulness of diffusion-weighted imaging in the evaluation of renal masses. AJR Am J Roentgenol 2010; 194:438–445. [CrossRef]
45. Jones TD, Eble JN, Cheng L. Application of molecular diagnostic techniques to renal epithelial neoplasms. Clin Lab Med 2005; 25:279–303. [CrossRef]
46. Lubensky IA, Schmidt L, Zhuang Z, et al. Hereditary and sporadic papillary renal carcinomas with c-met mutations share a distinct morphological phenotype. Am J Pathol 1999; 155:517–526. [CrossRef]
47. Pedrosa I, Chou MT, Ngo L, et al. MR classification of renal masses with pathologic correlation. Eur Radiol 2008; 18:365–375. [CrossRef]
48. Lesavre A, Correas JM, Merran S, Grenier N, Vieillefond A, Helenon O. CT of papillary RCCs with cholesterol necrosis mimicking angiomyolipomas. AJR Am J Roentgenol 2003; 181:143–145.
49. Grignon DJ, Eble JN. Renal neoplasms. In: Jennette JC, Olson JL, Schwartz MM, et al., eds. Heptinstall's pathology of the kidney. 6th ed. Philadelphia: Lippincott Williams & Wilkins, 2007; 1492–1531.
50. Pedrosa I, Sun MR, Spencer M. MR imaging of renal masses: correlation with findings at surgery and pathologic analysis. Radiographics 2008; 28:985–1003. [CrossRef]
51. Rosenkratz AB, Hindman N, Fitzgerald E, Niver BE, Melamed J, Babb JS. MRI features of renal oncocytoma and chromophobe RCC. AJR Am J Roentgenol 2010; 195:421–427. [CrossRef]
52. Srigley JR, Eble JN. Collecting duct carcinoma of the kidney. Semin Diagn Pathol 1998; 15:54–67.
53. Pickhardt PJ, Siegel CL, McLarney John K. Collecting duct carcinoma of the kidney: are imaging findings suggestive of the diagnosis? AJR Am J Roentgenol 2001; 176:627–633.
54. Pickhardt PJ, Lonergan GJ, Davis CJ, Kashitani N, Wagner BJ. Infiltrative renal lesions: radiologic-pathologic correlation. Radiographics 2000; 20:215–243.
55. Gurel S, Narra V, Gurel K, Chen ZM, Brown J. The role of magnetic resonance imaging in the radiological work-up of subtypes of renal cell carcinoma. Paper presented at 2005 Annual Meeting of the Radiological Society of North America, Chicago, Illinois, USA; November 27, 2004.
56. Murad T, Komaiko W, Oyasu R, Bauer K. Multilocular cystic RCC. Am J Clin Pathol 1991; 95:633–637.
57. Eble JN, Bonsib SM. Extensively cystic renal neoplasms: cystic nephroma, cystic partially differentiated nephroblastoma, multilocular cystic RCC and cystic hamartoma of renal pelvis. Semin Diagn Radiol 1998; 15:2–20.
58. Prasad SR, Humphrey PA, Catena JR, et al. Common and uncommon histologic subtypes of renal cell carcinoma: imaging spectrum with pathologic correlation. Radiographics 2006; 26:1795–1810. [CrossRef]
59. Hindman NM, Bosniak MA, Rosenkrantz AB, Lee-Felker S, Melamed J. Multilocular cystic RCC: comparison of imaging and pathologic findings. AJR Am J Roentgenol 2012; 198:20–26. [CrossRef]